Nield, Wiggs, Baddock, Hipondoka, Geology, accepted, uncorrected, author version
DOI:10.1130/G38800.1

Coupling leeside grainfall to avalanche characteristics in aeolian dune dynamics

Joanna M. Nield[1*], Giles F.S. Wiggs[2], Matthew C. Baddock[3], Martin H.T. Hipondoka[4]
[1]*Geography and Environment, University of Southampton, Southampton, SO171BJ, UK*
[2]*School of Geography and the Environment, University of Oxford, Oxford, OX13QY, UK*
[3]*Department of Geography, Loughborough University, Loughborough, LE113TU, UK*
[4]*Department of Geography, University of Namibia, Private Bag 13301, Windhoek, Namibia*
*E-mail: J.Nield@soton.ac.uk

ABSTRACT

Avalanche (grainflow) processes are fundamental drivers of dune morphodynamics and are typically initiated by grainfall accumulations. In sedimentary systems, however, the dynamism between grainfall and grainflow remains unspecified because simple measurements are hampered by the inherent instability of lee slopes. Here, for the first time, terrestrial laser scanning is used to quantify key aspects of the grainfall process on the lee (slipface) of a barchan sand dune. We determine grainfall zone extent and flux and show their variability under differing wind speeds. The increase in the downwind distance from the brink of peak grainfall under stronger winds provides a mechanism that explains the competence of large avalanches to descend the entire lee slope. These findings highlight important interactions between wind speed, grainfall, and subsequent grainflow that influence dune migration rates and are important for correct interpretation of dune stratigraphy.

INTRODUCTION

Avalanching or grainflow, where sediment accumulation from grainfall leads to exceedance of the repose angle and results in downslope transport by gravity, is a fundamental process in sedimentary bedform development. In aeolian environments, avalanching is the principal mechanism for dune dynamism, and the cross-strata which grainflows produce can provide a record of dune accumulation and formation. Broader insights taken from avalanche processes observed on sub-aerial dunes can also aid our understanding of bedforms in other geomorphic systems. For example, lee slope depositional processes are particularly problematic to measure in large fluvial systems where sediment transport is greatest close to the bed (Kostaschuk et al., 2009). In extra-terrestrial environments, interpretations of Martian aeolian wind patterns and dune activity have been derived from photographic evidence of dune leeside processes (Silvestro et al., 2010), where such analyses can only be enhanced by improved Earth analogue detail. Furthermore, avalanche deposits are a significant component of preserved aeolian stratigraphy, thus an understanding of avalanche processes provides important information for interpreting the rock record (Eastwood et al., 2012; Hunter, 1977).

Understanding leeside deposition processes is crucial for quantifying dune behavior, but until recently the instability and dynamic nature of these slopes have confounded detailed measurements of active processes. Technological advancements, particularly the development of terrestrial laser scanning (TLS), now permits non-disruptive, sequential, high resolution topographic surveying of unstable avalanche slopes, and allows quantification of morphological

change at the scale of individual avalanches. While insights have been gained into slope angle criticality and relaxation as well as sediment flux-avalanche frequency relationships both in laboratory (Sutton et al., 2013a; 2013b) and field settings (Pelletier et al., 2015), it is the dynamics of grainfall accumulation as a destabilizing process which ultimately triggers grainflow. Classic works have modeled (Anderson, 1988) and measured (Nickling et al., 2002) sediment fallout rates and their controls, but there have been no recent advances specifically relating to grainfall processes. This is despite such dynamics representing the connection between sand flux at the dune brink, lee-side avalanching dynamics, and dune migration.

In this field-based study, we employ new technology to make novel quantifications of the aeolian grainfall process and its relationship to avalanching. In doing so, we shed light on the fundamental drivers of leeside deposition on dunes and the geomorphological mechanisms that result in aeolian dune migration.

STUDY SITE AND METHODS

The Huab Valley dunefield in the Skeleton Coast National Park of NW Namibia consists of migratory barchan dunes responding to predominant S-SW winds (Hesp and Hastings, 1998; Lancaster, 1982). The avalanche dynamics on a lee slope of a migrating barchan were measured during periods of sand transport on the 4th and 5th September 2014. The dune (13.487°E, 20.869°S) was 5.12 m high, 95 m long, 69.5 m wide and had a slipface of 8 m horizontal length (Fig. 1).

Average wind speed was measured on the dune centerline 1.1 m upwind of the brink at an interval of 10 Hz using a Campbell C-SAT 3D sonic anemometer at 0.5 m height. Co-located saltation measurements (from which sand flux, Q_{Sz}, was calculated; Barchyn et al., 2014) were recorded at the same frequency using a Wenglor gate sensor at 0.02 m height.

Avalanche dynamics on the lee slope of the barchan were measured using a Leica P20 Scanstation TLS (resolution of 1.6 mm at 10 m), positioned 10 m downwind from the base of the lee slope along the dune centerline (Fig. 1). The TLS remained in place for the duration of the c. 3 h observations on each day with errors estimated at 3 mm (Hodge et al., 2009). We focused on a 3.4 m wide section of the lee slope adjacent to the brink instruments and dune centerline and perpendicular to the oncoming wind which took 46 s to scan. Measurements of the slope surface were repeated every 285 s. The TLS is able to detect saltating grains as partial signals above the slipface surface (Nield et al., 2011). This enables the quantification of the maximum length of travel of grains from the dune brink before being deposited on the lee slope as grainfall. Within each scan period, maximum grainfall length (i.e., the maximum horizontal downwind distance of grainfall above the lee slope) was determined as the maximum distance from the brink where one or more TLS point cloud measurements were detectable >0.025 m above the slope surface (Nield and Wiggs, 2011). This enabled an indication of the 95th percentile of grainfall length (GL_{95}) in 0.01 m across-slope bins for each period. The saltation flux (Q_{Sz}) over the brink was distributed by the 0.01 m binned grainfall frequency distribution to produce a horizontally distributed vertical grainfall flux (Q_G) characterized by the grainfall flux mode (Q_{Gm}).

Lee slope topographic change was quantified by differencing TLS measurements gridded at 0.01 m. Deposition rate (δ_D) for each period was determined from surface elevation change in the top 1 m of the slipface, for the areas where avalanching had not occurred further downslope. This specification eliminated any influence of avalanche-caused topographic change, surmounting a significant methodological issue raised by Pelletier et al. (2015).

RESULTS

Figure 2A shows strong positive exponential relationships between measured wind speed at the brink and both TLS-determined grainfall length (GL_{95}) and maximum grainfall distributed flux (Q_{Gm}) with R^2 values of 0.87 and 0.76 respectively. A strong nonlinear relationship is also seen between saltation flux at the brink (Q_{Sz}) and GL_{95} (R^2 0.89) (Fig. 2B). The plateauing of this curve reveals that at higher levels of Q_{Sz} (>2 kg m^{-2} s^{-1}), the GL_{95} does not increase downslope very rapidly, so that the increasing Q_{Gm} becomes more concentrated on the upper lee slope (within 1 m of the brink) as Q_{Sz} increases.

The deposition rate (δ_D) within the top 1 m of the lee slope also shows a strong positive and linear relationship with wind velocity (R^2 0.79) (Fig. 3A), while the decay of δ_D with distance from the brink is best represented by an exponential relationship (Fig. 3B). This measured decay in δ_D is comparable to values of deposition rate decay measured directly using flux samplers (Hunter, 1985; McDonald and Anderson, 1995; Nickling et al., 2002; Sutton et al., 2013b). Figure 3B also highlights the influence of windspeed on the shape of the decay curve with the location of the maximum value of δ_D shifting from 0.04 m to 0.06 m downwind of the brink as winds increase from <6 ms^{-1} to > 8 ms^{-1}.

The influence of windspeed on the characteristics of GL_{95} and Q_{Gm} is directly reflected in avalanche behavior. Figure 4A shows a surface change map of the lee slope between two scan periods during low wind (u = 5.2 ms^{-1}) with little saltation flux over the brink (Q_{Sz} = 0.13 $kgm^{-2}s^{-1}$). The calculated value of GL_{95} indicates that grainfall is focused within the top 0.21 m of the lee slope. Under such low wind speed (i.e., u <6 ms^{-1}), avalanche activity is typically characterized by the occurrence of small, discrete failures occurring close to the brink, with narrow necks (<0.34 m) and limited deposition lobe length (<2.14 m) and thickness (<0.018 m). Such avalanches produce small erosion zones (<0.59 m length) that are characteristic of the minimum accumulation that is capable of initiating avalanching. As mean wind speed, Q_{Gm} and GL_{95} increase, failures initiate further down the lee slope and larger avalanches become capable of reaching the bottom of the slipface (Fig. 4B; u = 6.5 ms^{-1}; GL_{95} = 0.32 m). Under strong winds (u = 8.4 ms^{-1}), avalanches occur as multiple families of failures, with primary avalanches at the top and secondary failures partway down the slope, resulting in the frequent descent of grainflows over the entire slope to the slipface base (Fig. 4C). GL_{95} in Figure 4C is 0.67 m and the erosion zone at the top of the slipface expands under these higher wind conditions. Maximum widths and lengths of eroded areas increased to 0.77 m and 1.92 m respectively for winds >6 ms^{-1}. Likewise, the deposition lobes also increased in length and thickness under these stronger winds (4.7 m and 0.03 m respectively).

The downslope extent of failure of the lee slope in changing wind conditions is shown in Figure 5A. For winds <6 ms^{-1}, the dominant mode of failure frequency was at 0.3 m, while for

>6 ms^{-1} the mode shifted further from the brink to 0.4 m, reaching as far as 1 m for winds >8 ms^{-1}. The maximum distance at which failures were detected for the lower velocity winds was 1.1 m, but Figure 5A shows that for winds >8 ms^{-1}, avalanche initiation occurred as far as 6.4 m from the brink. Figure 5B examines the location of avalanche initiation related to values of GL_{95} and confirms that failure points are close to the brink for low grainfall lengths (e.g, all avalanches originate within 1.35 m of the brink for GL_{95} <0.35 m) and the wide spread in failure locations associated with greater values of GL_{95}.

The grainfall downwind of the brink and the subsequent downslope grainflow activity leads to advancement of the slipface (Fig. 6A) and downwind dune migration but, crucially, migration only occurs when the avalanches reach as far as the base of the slipface. The importance of grainfall characteristics in the upper 1 m of the slipface in this process is demonstrated by the fact that GL_{95} emerges as a better predictor of slipface topographic change (R^2 0.9) than the saltation flux at the brink (Q_{Sz}) (R^2 0.85) (Fig. 6B).

DISCUSSION

While there is some ambiguity in the literature, we find a clear relationship between δ_D and wind speed (Fig. 3A, 3B). The resolution of the TLS allows us to offer the first field evidence identifying a peak in δ_D near the brink (Fig. 3B), supporting the modeling output of Anderson (1988). Significantly, our data also suggest a clear shift in the distance from the brink of this peak in δ_D as wind speed increases (from 0.04 for winds <6 ms^{-1} to 0.06 m for winds >8 ms^{-1}). This peak was not detected by Nickling et al. (2002) or Sutton et al. (2013b) possibly as a consequence of their leeside trap resolution and discretization.

A central issue of contention in linking grainfall to dune migration rate relates to the significance of wind speed as a driver of avalanche volume. Sutton et al. (2013a) reported no relationship between these variables in laboratory experiments and suggested that avalanche frequency, rather than magnitude increases with wind speed, supporting the results of McDonald and Anderson (1996) and Breton et al. (2008). While our data show a similar disconnect between wind speed and net surface change within the top 1 m of the lee slope (where surface change includes both grainfall and grainflow), we do find that net surface change scales well with wind speed across the whole slipface (power exponent 6.5; R^2 0.9; Fig. 6A). It is notable, however, that the shape of the curve in Figure 6A illustrates negligible net surface change of the lee slope at low wind speeds (<6 ms^{-1}).

While our data confirm an increase in avalanche frequency under stronger winds (Fig. 5), we also observed an increase in avalanche magnitude (both volume and extent; Fig. 4). Identifying drivers of avalanche magnitude is important because deposit thickness is crucial for interpreting dune stratigraphy (Anderson, 1988; McDonald and Anderson, 1996). The increase in avalanche magnitude with increasing windspeed in our study is indicated by the appearance of grainflows that descend the entire lee slope, with deposition lobes which expand both in width (0.4 m to 1.13 m for u >6 ms^{-1}) and depth (0.018 m to 0.03 m; e.g., Figure 4B and C) when wind speeds exceed 6 ms^{-1}.

Our data therefore suggest that some caution should be exercised in using wind speed as a simple driver for dune migration rate. This is because at low wind speeds the value of GL_{95} is small and the location of Q_{Gm} is close to the brink (Figs. 2A and 3A). Low wind speeds trigger small avalanches which diminish within 1–2 m of travel (Fig. 4A) resulting in no net migration of the dune. In contrast, at high windspeeds the value of GL_{95} increases (maximum GL_{95} = 0.75 m) and the location of Q_{Gm} moves further downslope (Fig. 3B) resulting in a greater proportion of sediment being delivered further from the brink. This allows for the destabilization of a larger area of the lee slope because of the increased contribution to the avalanche from sediment destabilized above the point of failure (McDonald and Anderson, 1996; Sutton et al., 2013a). High windspeeds therefore trigger proportionally larger avalanche failures (Fig. 4C) than low windspeeds. Further, the existence of failures outside the grainfall zone (Fig. 5A) suggests that in high windspeeds secondary avalanches are also initiated further downslope in response to accumulation of sediment resulting from the primary avalanches on the upper slopes (e.g., McDonald and Anderson, 1996; Sutton et al., 2013a). Sediment delivery from these primary avalanches forms additional 'bulges' of deposition as far as 6.4 m from the brink, which eventually fail and move additional sediment to the slipface base.

At high wind speeds dune migration rate is therefore intensified nonlinearly in comparison to lower windspeed conditions due to a) higher values of brink saltation driven by the higher windspeeds, b) larger avalanche failures caused by the downslope shift in peak grainfall flux and, c) the triggering of secondary avalanche failures further down the slipface. The variability of the proportion of the slipface affected by grainfall is therefore a key control on avalanche dynamics and dune migration rate. Further, the limited morphological impact on the dune lee slope caused by low wind conditions is likely to be obliterated by the large scale morphological change induced in high wind conditions, the concept of sedimentary signal shredding (Jerolmack and Paola, 2010). The restriction of avalanches to the upper slopes of the slipface in low wind speed conditions, together with sedimentary signal shredding, implies that the aeolian signature of low energy conditions in a dune environment is unlikely to be well-represented in dune stratigraphy and may be very difficult to resolve from the rock record (e.g., Eastwood et al., 2012). It also suggests that along with dune height (Kocurek and Dott, 1981), wind speed is an important driver of deposit stratigraphic thickness.

CONCLUSIONS

In combining airflow and sand transport measurements with high frequency TLS this work offers a new approach for quantifying grainfall, one of the fundamental and most persistently poorly understood processes of deposition on aeolian dunes. For the first time, this field study identifies the process of grainfall zone expansion with increasing wind speed and recognizes its crucial role in intensifying avalanche dynamics on aeolian lee slopes. Our data indicate that a nonlinearity exists between wind speed and the magnitude of lee slope avalanching such that the imprint of low wind conditions on dune migration dynamics are unlikely to be preserved in dune stratigraphy. Such low energy conditions may therefore be under-represented in interpretations of the rock record.

ACKNOWLEDGMENTS

This study was funded by National Geographic Society Science and Exploration Europe (GEFNE110–14), British Society for Geomorphology and NERC GEF (1025) grants. Data processing used IRIDIS Southampton Computing Facility. We thank the Namibia Ministry of Environment and Tourism, I. Matheus, J. Kazeurua and Skeleton Coast National Park Rangers (permit 1913/2014), J. Mayaud, M. David, S. Muinjo, B. Shiyanga, D. Beben, T. Bishop and W. Nickling for field and instrument assistance. J. Schmitt, N. Lancaster, S. Sutton and anonymous reviewer are thanked for helping improve this manuscript.

REFERENCES CITED

Anderson, R.S., 1988, The pattern of grainfall deposition in the lee of aeolian dunes: Sedimentology, v. 35, p. 175–188, doi:10.1111/j.1365-3091.1988.tb00943.x.

Barchyn, T.E., Hugenholtz, C.H., Li, B., Neuman, C.M., and Sanderson, R.S., 2014, From particle counts to flux: Wind tunnel testing and calibration of the Wenglor aeolian sediment transport sensor: Aeolian Research, v. 15, p. 311–318, doi:10.1016/j.aeolia.2014.06.009.

Breton, C., Lancaster, N., and Nickling, W.G., 2008, Magnitude and frequency of grain flows on a desert sand dune: Geomorphology, v. 95, p. 518–523, doi:10.1016/j.geomorph.2007.07.004.

Eastwood, E.N., Kocurek, G., Mohrig, D., and Swanson, T., 2012, Methodology for reconstructing wind direction, wind speed and duration of wind events from aeolian cross-strata: Journal of Geophysical Research. Planets, v. 117, p. F03035.

Hesp, P.A., and Hastings, K., 1998, Width, height and slope relationships and aerodynamic maintenance of barchans: Geomorphology, v. 22, p. 193–204, doi:10.1016/S0169-555X(97)00070-6.

Hodge, R., Brasington, J., and Richards, K., 2009, In situ characterization of grain-scale fluvial morphology using terrestrial laser scanning: Earth Surface Processes and Landforms, v. 34, p. 954–968.

Hunter, R.E., 1977, Basic types of stratification in small eolian dunes: Sedimentology, v. 24, p. 361–387, doi:10.1111/j.1365-3091.1977.tb00128.x.

Hunter, R.E., 1985, A Kinematic model for the structure of lee-side deposits: Sedimentology, v. 32, p. 409–422, doi:10.1111/j.1365-3091.1985.tb00520.x.

Jerolmack, D.J., and Paola, C., 2010, Shredding of environmental signals by sediment transport: Geophysical Research Letters, v. 37, L19401, doi:10.1029/2010GL044638.

Kocurek, G., and Dott, R.H.J., 1981, Distinctions and uses of stratification types in the interpretation of eolian sand: Journal of Sedimentary Petrology, v. 51, p. 579–595.

Kostaschuk, R., Shugar, D., Best, J., Parsons, D., Lane, S., Hardy, R., and Orfeo, O., 2009, Suspended sediment transport and deposition over a dune: Rio Parana, Argentina: Earth Surface Processes and Landforms, v. 34, p. 1605–1611, doi:10.1002/esp.1847.

Lancaster, N., 1982, Dunes on the Skeleton Coast, Namibia (South West-Africa) - geomorphology and grain-size relationships: Earth Surface Processes and Landforms, v. 7, p. 575–587, doi:10.1002/esp.3290070606.

McDonald, R.R., and Anderson, R.S., 1996, Constraints on eolian grain flow dynamics through laboratory experiments on sand slopes: Journal of Sedimentary Research, v. 66, p. 642–653.

McDonald, R.R., and Anderson, R.S., 1995, Experimental verification of aeolian saltation and lee side deposition models: Sedimentology, v. 42, p. 39–56, doi:10.1111/j.1365-3091.1995.tb01270.x.

Nickling, W.G., Neuman, C.M., and Lancaster, N., 2002, Grainfall processes in the lee of transverse dunes, Silver Peak, Nevada: Sedimentology, v. 49, p. 191–209, doi:10.1046/j.1365-3091.2002.00443.x.

Nield, J.M., and Wiggs, G.F.S., 2011, The application of terrestrial laser scanning to aeolian saltation cloud measurement and its response to changing surface moisture: Earth Surface Processes and Landforms, v. 36, p. 273–278, doi:10.1002/esp.2102.

Nield, J.M., Wiggs, G.F.S., and Squirrell, R.S., 2011, Aeolian sand strip mobility and protodune development on a drying beach: Examining surface moisture and surface roughness patterns measured by terrestrial laser scanning: Earth Surface Processes and Landforms, v. 36, p. 513–522, doi:10.1002/esp.2071.

Pelletier, J.D., Sherman, D.J., Ellis, J.T., Farrell, E.J., Jackson, N.L., Li, B., Nordstrom, K.F., Maia, L.P., and Omidyeganeh, M., 2015, Dynamics of sediment storage and release on aeolian dune slip faces: A field study in Jericoacoara, Brazil: Journal of Geophysical Research, Earth Surface, v. 120, p. 1911–1934, doi:10.1002/2015JF003636.

Silvestro, S., Fenton, L.K., Vaz, D.A., Bridges, N.T., and Ori, G.G., 2010, Ripple migration and dune activity on Mars: Evidence for dynamic wind processes: Geophysical Research Letters, v. 37, L20203, doi:10.1029/2010GL044743.

Sutton, S.L.F., McKenna Neuman, C., and Nickling, W., 2013a, Avalanche grainflow on a simulated aeolian dune: Journal of Geophysical Research, Earth Surface, v. 118, p. 1767–1776, doi:10.1002/jgrf.20130.

Sutton, S.L.F., McKenna Neuman, C., and Nickling, W., 2013b, Lee slope sediment processes leading to avalanche initiation on an aeolian dune: Journal of Geophysical Research, Earth Surface, v. 118, p. 1754–1766, doi:10.1002/jgrf.20131.

DOI:10.1130/G38800.1

FIGURES

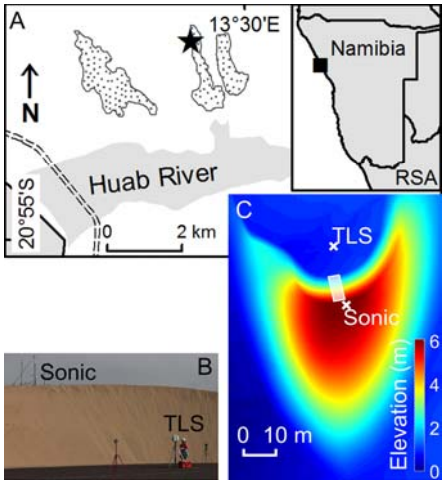

Figure 1. (A) Huab location within Namibia and map of study site, with dune location marked by star. Stippled areas indicate areas of barchan and other aeolian deposits constituting the Huab dunefield. (B) Lee slope experimental set-up. (C) DEM of study barchan with placement of sonic anemometer and TLS. The scanned area is indicated by the shaded rectangle.

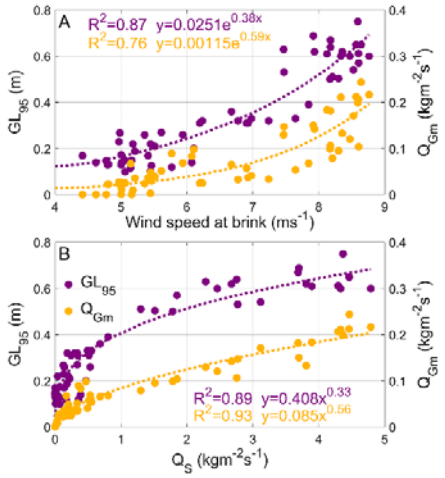

Figure 2. Comparison of (A) wind speed and (B) saltation flux measured at the brink (Q_{Sz}) to 95th percentile of measured grainfall length (GL_{95}) and maximum value of the derived grainfall flux (Q_{Gm}) on the lee slope.

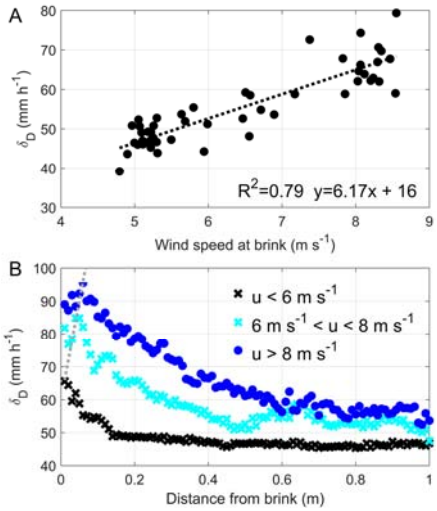

Figure 3. (A) Mean deposition flux (δ_D) within the top 1 m of lee slope for the range of measured wind speeds, (B) Variation in deposition flux with horizontal distance from the brink averaged for all runs within each of three different wind speed categories (<6 ms^{-1}, 6–8 ms^{-1}, >8 ms^{-1} where n = 27, 10 and 14 respectively). Dashed line links position of peak δ_D at different wind speeds.

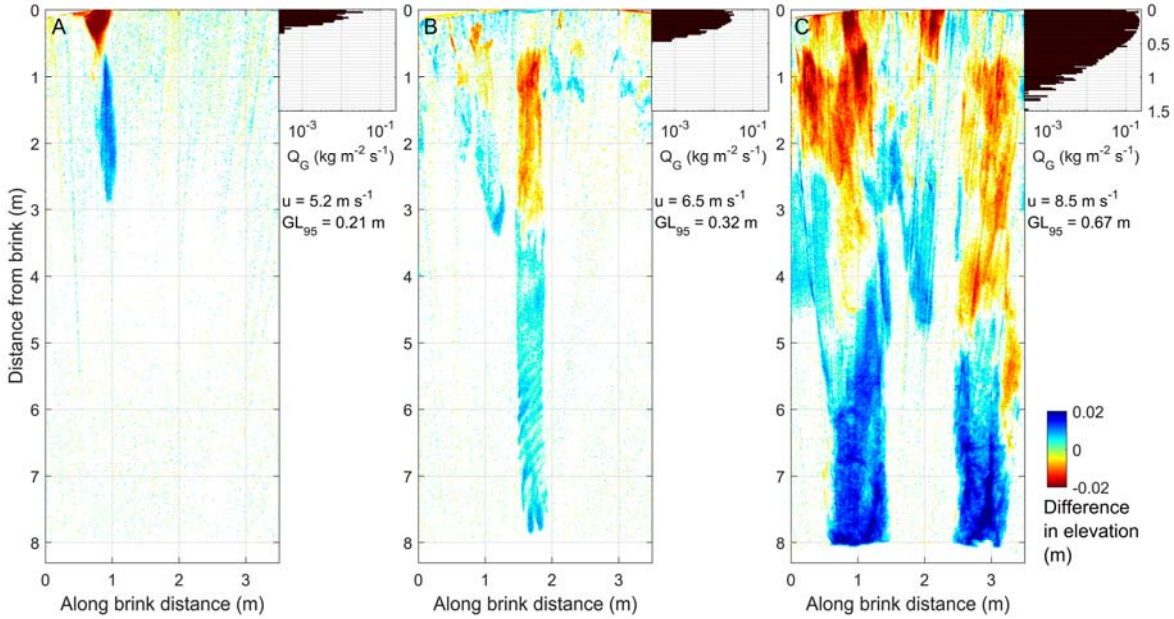

Figure 4. Examples of typical change in surface elevation between sequential scans, illustrating avalanche behavior, under conditions of (A) low, (B) intermediate and (C) high mean wind speeds. Also shown aligned with vertical scale is frequency histogram of derived grainfall flux distribution (Q_G; log scale on *x* axis) for each case. See supplementary data for animation of avalanches for each of the 51 scan periods.

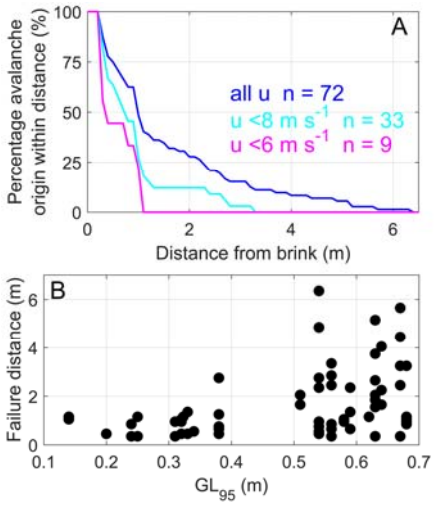

Figure 5. (A) Cumulative frequency of detected point of avalanche origin with distance from the brink, including subsets of wind speeds below 6 ms^{-1} (magenta) and 8 ms^{-1} (cyan). (B) Distance from brink of avalanche initiation (failure distance) as a function of maximum grainfall length (GL_{95}).

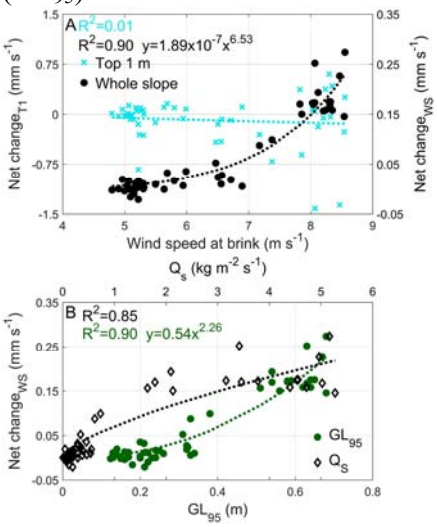

Figure 6. (A) Rate of net surface height change (including grainfall and grainflow affected areas) for each scan period for both the top 1 m of the lee slope (T1) and the whole of the lee slope (WS), as a function of wind speed. (B) Rate of net surface height change across the whole of the lee slope as a function of maximum grainfall length (GL_{95}, bottom *x*-axis) and saltation flux at the brink (Q_{Sz}, top *x*-axis).

GSA Data Repository item 201Xxxx, [additional methods and animations], is available online at www.geosociety.org/pubs/ft20XX.htm, or on request from editing@geosociety.org or Documents Secretary, GSA, P.O. Box 9140, Boulder, CO 80301, USA.

Nield, Wiggs, Baddock, Hipondoka, Geology, accepted, uncorrected, author version
DOI:10.1130/G38800.1

Supplementary material for: Nield et al., Coupling leeside grainfall to avalanche characteristics in aeolian dune dynamics, for submission to Geology.

Supplementary location, methods and results, including animations:

The study dune was the largest bedform at the downwind end of a train of barchan dunes, emerging from the Huab Valley, Namibia (Fig. S1). The migration rate measured in the year subsequent to the avalanche study was approximately 22 ma^{-1}. Mean grain size for sediment sampled at the brink of the study dune was 261 μm.

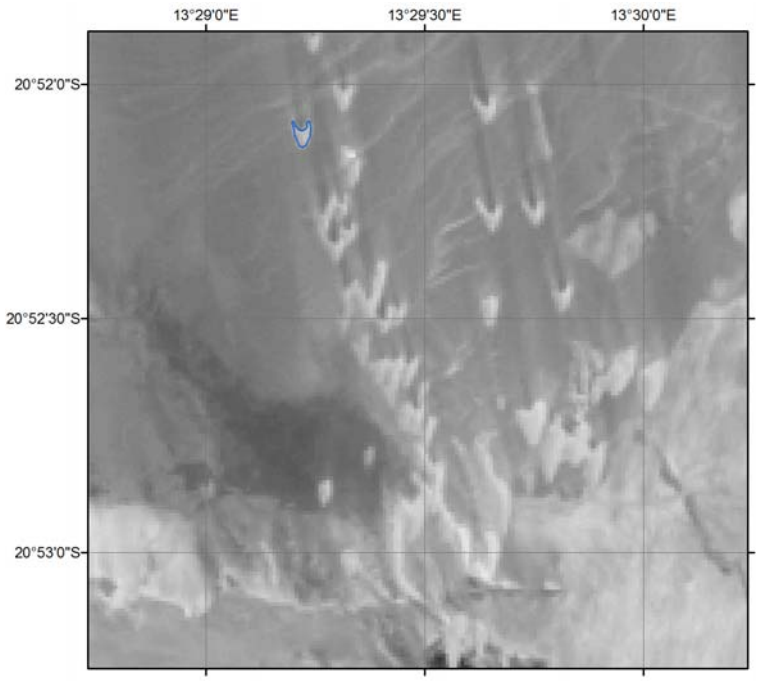

Figure S1: Landsat 8 Band 8 image of the Huab dune train from 3rd September 2014, with the study barchan outlined in blue. See supplementary Animation 1 of raw TLS data in three dimensions for our study dune.

As well as the airflow and saltation flux measurements made 1.1 m upwind of the dune brink which were directly pertinent to our experiment, 10 s average wind speed and direction were also recorded in the unperturbed flow 75 m upwind of the study barchan at a height of 1.5 m using a Gill 2D Windsonic anemometer. The wind direction measured at this location confirmed a consistent wind direction throughout the experiment duration (Fig. S2).

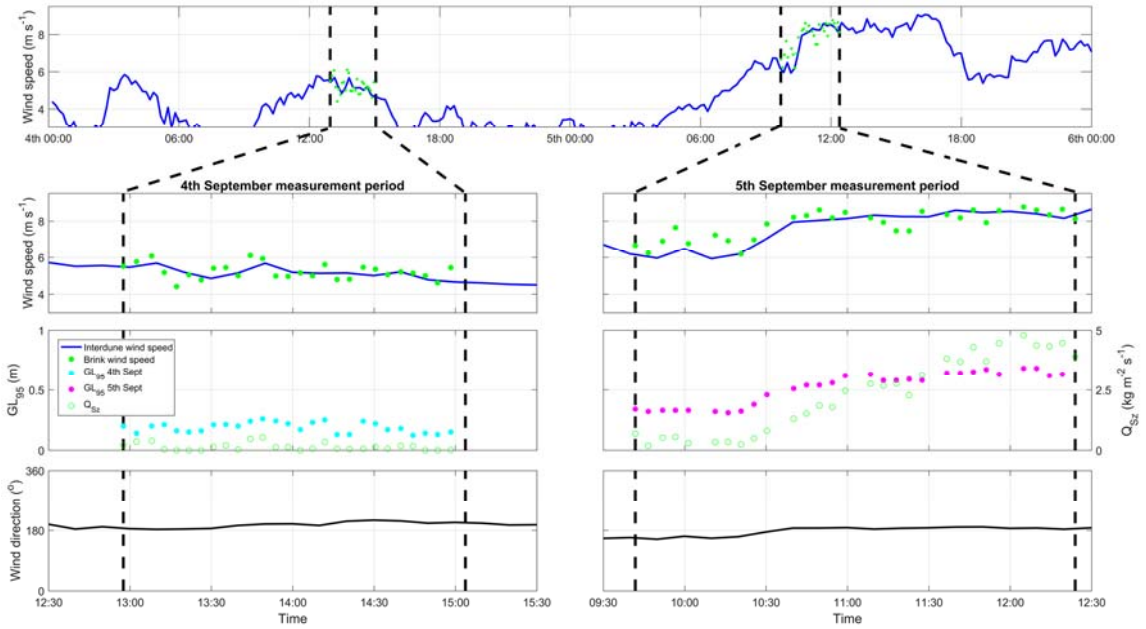

Figure S2: Wind and sand transport conditions during the experiment measurement periods (dashed lines) on the 4th and 5th September 2014.

Three different methods were used to measure or derive different aspects of sediment flux and deposition rate in this study (Fig. S3). First, Wenglor instruments located on the brink of the dune measured saltation flux rates. Second, TLS detection of grains above the surface, downwind of the brink (i.e. the grainfall population of sand), was used to quantify the horizontal grainfall zone (the dashed line in Fig. S3B). This detection was undertaken over a 46 s period, which enabled a distribution of maximum grain travel distance from the brink to be collected for each 0.01 m across-slope bin during the measurement period. An example of the binned data is illustrated in Fig. S4. The measured Q_{Sz}, spatially distributed within the horizontal grainfall zone was then used to determine the magnitude, of the mode of this distributed flux (Q_{Gm}). Finally, vertical deposition rates, δ_D, (similar to the lower boom cup measurements of Nickling et al. (2002)), were calculated directly from TLS topographic surface measurements.

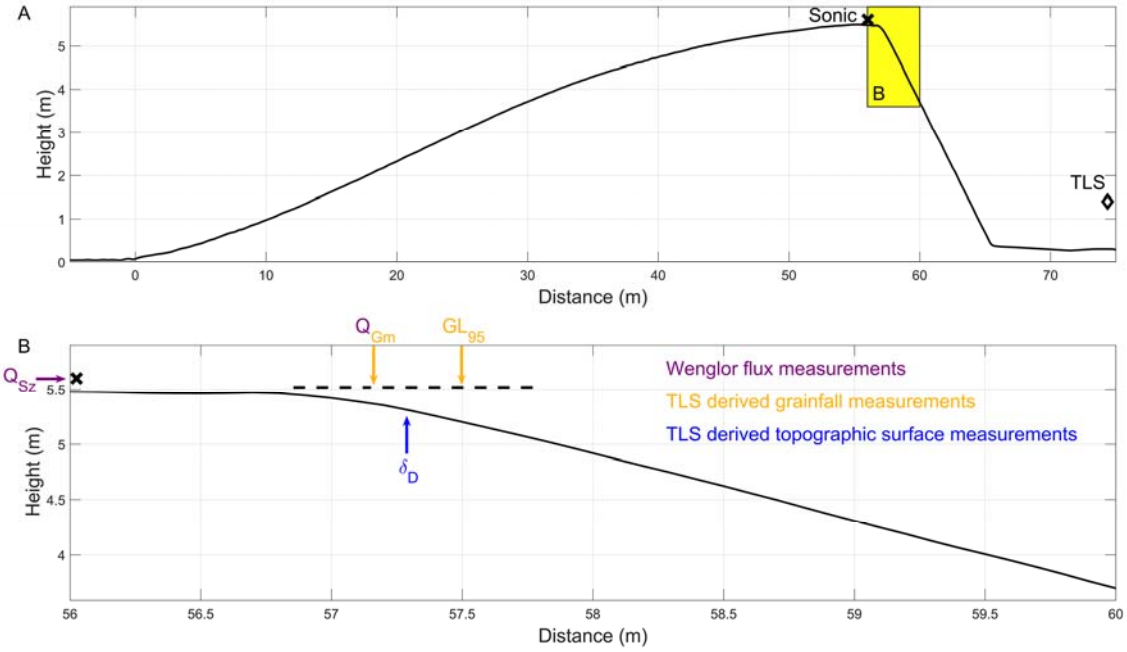

Figure S3: (A) Centreline of study barchan with location of sonic anemometer and Wenglor instrumentation marked with a cross and TLS marked with a diamond. Yellow box indicates area enlargement in B. (B) Indication of measurements made near and downwind of the dune brink and the relationships of each of the measurements discussed within this study, i.e. saltation flux (Q_{Sz}), modal grainfall flux (Q_{Gm}), 95th percentile of grainfall length (GL_{95}) and deposition rate (δ_D).

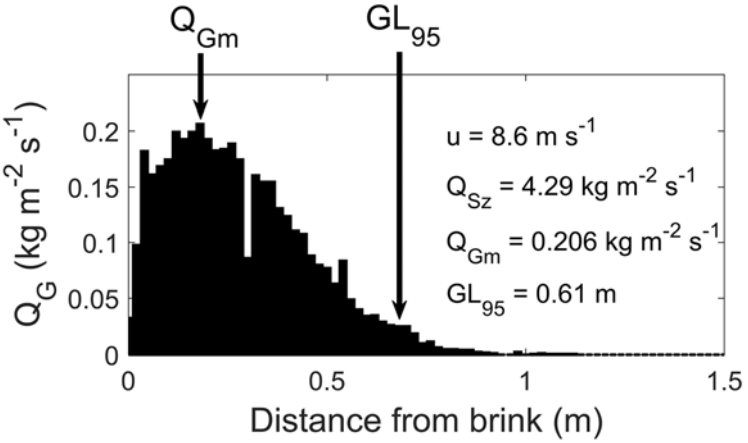

Figure S4: Nomenclature for TLS derived grainfall measurements for a single example scan period of measured wind speed (u) and saltation flux (Q_{Sz}).

For quantification of topographic change and avalanche dynamics on the dune lee slope a minimum height for change detection of 0.003 m was applied in order to eliminate measurement noise. This value is in agreement with typical Leica internal detection errors (e.g., Hodge et al., 2009). Avalanche origin (the initiation point of slope failure) was then derived from the point of

maximum change in slope angle between two subsequent scans within identified erosion scarps (Table S1).

Avalanche behaviour varied depending on the wind velocity (u), and we have divided our results into low, medium and high categories for $u < 6$ ms^{-1}, 6 ms^{-1} $< u < 8$ ms^{-1} and $u > 8$ ms^{-1} respectively. Values of the mean, standard deviation and range of avalanche size characteristics for each of these categories are presented in Table S1. For the full set of spatial behaviours and the transport conditions measured, see Animation 2.

Nield, Wiggs, Baddock, Hipondoka, Geology, accepted, uncorrected, author version
DOI:10.1130/G38800.1

Table S1 Measured avalanche dimensions for different wind speed groups

			Wind speed category			
			u <6 ms^{-1}	u >6 ms^{-1}	u <8 ms^{-1}	u >8 ms^{-1}
Erosion scarp	Length (m)	Mean	0.40	0.71	0.68	0.60
		Standard deviation	0.13	0.45	0.50	0.26
		Minimum	0.21	0.24	0.21	0.24
		Maximum	0.59	1.92	1.92	1.03
	Width (m)	Mean	0.23	0.35	0.34	0.29
		Standard deviation	0.07	0.16	0.18	0.10
		Minimum	0.16	0.11	0.11	0.12
		Maximum	0.34	0.77	0.77	0.43
	Thickness (m)	Mean	0.0005	0.0033	0.0016	0.0050
		Standard deviation	0.0040	0.0038	0.0044	0.0012
		Minimum	0.0000	0.0000	0.0000	0.0031
		Maximum	0.0055	0.0075	0.0075	0.0063
Deposition Lobe	Length (m)	Mean	1.19	1.09	1.17	1.07
		Standard deviation	0.58	0.77	0.68	0.79
		Minimum	0.54	0.22	0.40	0.22
		Maximum	2.14	4.70	3.16	4.70
	Width (m)	Mean	0.30	0.37	0.38	0.36
		Standard deviation	0.08	0.20	0.20	0.19
		Minimum	0.18	0.13	0.13	0.13
		Maximum	0.40	1.13	1.10	1.13
	Thickness (m)	Mean	0.0149	0.0154	0.0155	0.0153
		Standard deviation	0.0026	0.0035	0.0034	0.0035
		Minimum	0.0116	0.0100	0.0115	0.0100
		Maximum	0.0181	0.0303	0.0280	0.0303

Nield, Wiggs, Baddock, Hipondoka, Geology, accepted, uncorrected, author version
DOI:10.1130/G38800.1

Supplementary Animations:

Animation 1 (animation1.avi): Three dimensional representation of the study dune, based on raw TLS point cloud data. Sonic anemometer and Wenglor measurement location highlighted by the colour tower on the dune brink. Flythrough ends with a close-up of the lee slope where experiments were undertaken. File size is ~35MB.

Animation 2 (animation1.avi): Avalanche behavior (surface change of the lee slope) for each of the 51 measurement periods, ordered by increasing mean wind speed of scan period (i.e., not ordered in time). Surface change is indicated on left. Also shown aligned with vertical scale is frequency histogram of derived grainfall flux distribution (Q_G; log scale on x axis) for each case. Wind speed (u) and 95th percentile distributions of grainfall length (GL_{95}) are indicated on the bottom right for each measurement period. See Fig. 3 for examples of avalanche behavior under conditions of (A) low, (B) intermediate and (C) high mean wind speeds. File size is ~2 MB.